JOURNAL OF AGRICULTURAL AND FOOD CHEMISTRY

pubs.acs.org/JAFC Article

Role of Foliar Biointerface Properties and Nanomaterial Chemistry in Controlling Cu Transfer into Wild-Type and Mutant *Arabidopsis thaliana* Leaf Tissue

Yu Shen, Jaya Borgatta, Chuanxin Ma, Gurpal Singh, Carlos Tamez, Neil P. Schultes, Zhiyun Zhang, Om Parkash Dhankher, Wade H. Elmer, Lili He, Robert J. Hamers,* and Jason C. White*

Cite This: https://doi.org/10.1021/acs.jafc.1c07873 Read Online

ACCESS | Metrics & More | Article Recommendations | Supporting Information

ABSTRACT: Seven *Arabidopsis thaliana* mutants with differences in cuticle thickness and stomatal density were foliar exposed to 50 mg L^{-1} $Cu_3(PO_4)_2$ nanosheets (NS), CuO NS, CuO nanoparticles, and $CuSO_4$. Three separate fractions of Cu (surface-attached, cuticle, interior leaf) were isolated from the leaf at 0.25, 2, 4, and 8 h. Cu transfer from the surface through the cuticle and into the leaf varied with mutant and particle type. The Cu content on the surface decreased significantly over 8 h but increased in the cuticle. Cu derived from the ionic form had the greatest cuticle concentration, suggesting greater difficulty in moving across this barrier and into the leaf. Leaf Cu in the increased-stomatal mutants was 8.5−44.9% greater than the decreased stomatal mutants, and abscisic acid to close the stomata decreased Cu in the leaf. This demonstrates the importance of nanomaterial entry through the stomata and enables the optimization of materials for nanoenabled agriculture.

KEYWORDS: *Cu nanomaterials, cuticle, stomata, Arabidopsis, hydrophobic surface*

■ INTRODUCTION

Given the projected pressure on agriculture from an increasing population and a changing climate, nanotechnology has garnered significant attention as a potentially critical tool for maximizing global food production and achieving food security.[1,2] Current potential applications have included nanoscale platforms for nutrient delivery, plant protection strategies for pathogen management, the development of intelligent nanoscale sensing systems for a range of parameters, and strategies to increase photosynthesis or even tolerance to stress, among other uses.[3−5] A number of studies have focused specifically on the foliar application of a range of nanoparticles as a method to improve crop production and resistance to pathogens. For example, Nandhini et al. reported that the foliar application of 50 mg L^{-1} zinc oxide nanoparticles (ZnO NPs) to pearl millet resulted in a 35% reduction in downy mildew (*Sclerospora graminicola*) incidence compared to untreated controls; 250 mg L^{-1} ZnO increased seedling vigor by 71.5%.[6] Buchman et al. demonstrated that foliar application of 500 mg L^{-1} chitosan-coated mesoporous Si NPs reduced *Fusarium* wilt disease by 27% in a greenhouse study with watermelon and under field conditions, increased the fruit yield of watermelon by 70%.[7] Our group has focused significant attention on the role of nanoscale Cu in modulating plant health and resistance to disease.[8−12] For example, Borgatta et al. found that foliar application of $Cu_3(PO_4)_2{\cdot}3H_2O$ nanosheets to 2 week old seedlings increased the mass of individual watermelon fruit by 38.2% under *Fusarium*-infested conditions.[13] Similarly, Ma et al. demonstrated that foliar application of nanoscale Cu in different forms could effectively suppress soybean sudden death syndrome (SDS) caused by *Fusarium virguliforme,* and importantly, nanomaterial affinity to the leaf surface and dissolution of Cu ions could be modeled computationally.[9] This previous work has clearly demonstrated that nanomaterial attachment to and movement through the leaf biointerface is critical to the observed plant benefits; understanding of the important interactions between nanomaterial chemistry and leaf surface chemistry is lacking.

The leaf biointerface is a complex framework of epidermal cells and varied structures such as the cuticle, stomata, and trichomes that forms a hydrophobic barrier between the outer environment and the inner leaf tissue. The leaf surface itself is covered with a waxy cuticle which is impermeable to liquid water and water vapor and chemically consists of a wide range of organic compounds such as palmitic acid, stearic acids, octacosanol, and hentriacontane.[14] Permeated through the cuticle are stomata, which are 3−10 μm pores that regulate the exchange of gases and water vapor between the outside atmosphere and the interior of the leaf, including mesophyll and vascular tissues.[15,16] Importantly, the mechanistic role of specific leaf structures in the transfer of nanoscale materials and/or dissolved ions from the foliar surface to the leaf interior is not well understood. The foliar surface free energy (SFE) is a quantitative measure of the polar and dispersive surface forces of the leaf and is a function of leaf thickness and the

Received: December 9, 2021
Revised: March 24, 2022
Accepted: March 24, 2022

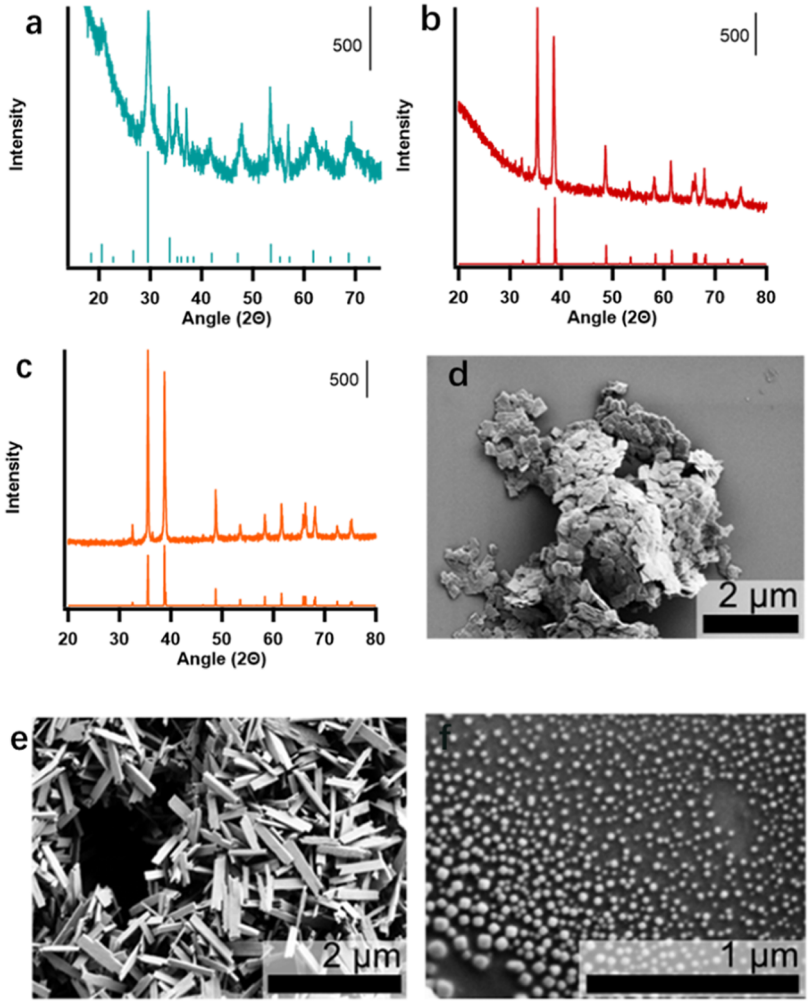

Figure 1. X-ray diffraction patterns of $Cu_3(PO_4)_2$ nanosheets (a), CuO nanosheets (b), and commercial CuO nanoparticles (c) and scanning electron microscopy (SEM) images of $Cu_3(PO_4)_2$ nanosheets (d), CuO nanosheets (e), and commercial CuO nanoparticles (f) at a scale of 1000 nm.

distribution and functionality of surface structures. The SFE can roughly be viewed as an indicator of overall surface hydrophobicity/hydrophilicity; plants with low SFE have been reported as being significantly more likely to adhere and retain NPs than plants with higher SFE values.[17] Although SFE speaks directly to particle attachment, mechanisms of particle entry into the leaf are largely uncharacterized. Eichert et al. suggested that plants absorbed liquid NH_4^+ or NO_3 through the stomatal pores as opposed to the cuticle pathway.[18] Similarly, Wang et al. hypothesized that nanoparticles of Fe_2O_3, TiO_2, MgO, and ZnO entered the leaf through the stomatal pathway; NP presence was subsequently confirmed through the leaf stomata by transmission electron microscopy.[19] Avellan et al. demonstrated the importance of chemical coating to particle accumulation by showing that negatively charged citrate-Au NPs were more likely to be retained on the outer cuticle layer of wheat leaves after 2 weeks, whereas positively charged poly(vinylpyrrolidone) (PVP)−Au NPs much more effectively crossed the cuticle.[20] Similarly, Hu et al. observed that positively charged (>15 mV) hydrophilic cerium oxide (CeO_2) and silica (SiO_2) nanoparticles (<20 nm) exhibited more effective transfer through the leaf tissues of cotton and corn than did carbon dots.[21] Shen et al. compared the movement of ionic and nanoscale Cu across tomato leaves over 8 h and found that the nanoscale forms were accumulated in the leaf tissue to a significantly greater extent, with the $CuSO_4$ foliar application leading to 7-fold greater Cu retention in the cuticle layer. Importantly, this greater intraplant accumulation of Cu with the nanoscale treatment led to increased resistance to the root pathogen *Fusarium oxysporum f. sp. lycopersici*. However, studies comparing the role of the cuticle and stomata in controlling nanoparticle movement across the plant leaf biointerface are limited, but it is clear that a mechanistic understanding of this process is critical to the success of nanoenabled foliar amendment strategies.

To jointly investigate the role of both leaf surface and Cu nanomaterial properties in particle accumulation, CuO nanosheets, CuO nanoparticles, $Cu_3(PO_4)_2{\cdot}3H_2O$ nanosheets, and $CuSO_4$ were foliarly applied at 50 mg L^{-1} total Cu to the leaves of wild-type *Arabidopsis* spp., as well as to mutants with increased- or decreased-cuticle thickness, or decreased- or increased-stomatal activity. The time-dependent distributions of Cu in the surface-attached, cuticle, and interior leaf fractions of *Arabidopsis thaliana* leaves were assessed over 8 h. Although this approach does not tell us the form of Cu in these fractions, this design does enable an assessment of not only the role of nanomaterial morphology and dissolution profile in Cu accumulation but also a determination of the most important

https://doi.org/10.1021/acs.jafc.1c07873
J. Agric. Food Chem. XXXX, XXX, XXX−XXX

pathway of uptake: stomata or cuticle. This work increases our basic understanding of nanomaterial accumulation across this important biological interface in the environment and will be useful in optimizing the design of nanoscale agrochemicals for controllable accumulation as part of sustainable nanoenabled agriculture.

■ MATERIALS AND METHODS

Materials Properties. CuO nanosheets were prepared by a hydrothermal microwave synthesis method (Section S1). $Cu_3(PO_4)_2 \cdot 3H_2O$ nanosheets were synthesized and characterized as reported previously.[8] Commercial nanoscale CuO (30 nm diameter; powder, CuO nanoparticles) was purchased from U.S. Research Nanomaterials (Houston, TX). Copper chloride dihydrate, ammonium phosphate monobasic, and diethylene glycol were obtained from Sigma-Aldrich (St. Louis, MO); all reagents were used as purchased. In the foliar exposure experiments described below, the CuO nanosheets (NS), CuO nanoparticles (NPs), and $Cu_3(PO_4)_2 \cdot 3H_2O$ (NS) were applied by mass concentration (mg L^{-1}). However, the concentrations added were adjusted based on individual stoichiometries to ensure equivalent doses of Cu; specifically, CuO and $Cu_3(PO_4)_2 \cdot 3H_2O$ are 85 ± 6 and 44 ± 4% mass percent Cu, respectively.[8,9] Additional information on material synthesis and subsequent characterization by SEM, XRD, and a zetasizer are described in Figures 1 and S4. Importantly, this suite of materials represents different morphologies and compositions that allow us to effectively probe the role of nanomaterial chemistry on attachment to and movement across the leaf biointerface. Cu^{2+} release from commercial CuO NPs, CuO, and $Cu_3(PO_4)_2$ were evaluated in deionized water, and Cu concentrations were determined by inductively coupled plasma-mass spectrometry (ICP-MS, Agilent 7500ce, Santa Clara, CA) as described in Section S1.

Plant Growth and Nanomaterial Exposure. *A. thaliana* seeds were purchased from the Arabidopsis Biological Resource Center (ABRC). We selected the following *Arabidopsis* lines: wild type (*Col-0*), homozygous T-DNA mutants with a decreased/compromised cuticle (SALK_032531; "decreased cuticle"), two mutants with altered cuticle (SALK_036774 and SALK_121760; "increased cuticle"), several mutants with decreased stomatal activity (seed line CS67139 containing homozygous SALK_047918 and SALK_137549 mutations and SALK_134698; "decreased stomata"), and a mutant with increased-stomatal activity (SALK_106556; "increased stomata") (Table S1). *A. thaliana* seeds were surface sterilized with 70% (v/v) ethanol for 5 min, followed by 30% commercial bleach (Clorox; containing 6% sodium hypochlorite) for 30 min. The seeds were then washed four times with autoclaved deionized H_2O. Fifty sterilized seeds were placed on Petri dishes and transferred to 4 °C for 24 h for vernalization. After vernalization, the Petri dishes were moved to a controlled environment cabinet (Percival Scientific, Perry, IA) with 16 h light and 8 h dark at 22 and 18 °C for 14 days, respectively. *A. thaliana* seedlings were transferred to 450 mL plastic pots with the Pro-Mix BX soil (Premier Horticulture Inc., PA); the seedlings were fertilized with 20 mL of Peter's soluble 20−10−20 (N−P−K) fertilizer (R.J. Peters, Inc., Allentown, PA) every 7 days. The seedlings grew under controlled conditions (day/night temperature of 25/20 °C and relative humidity of 65%) in the greenhouse of the College of Natural Science at the University of Massachusetts, Amherst.

For the foliar exposure, 114.2 mg L^{-1} $Cu_3(PO_4)_2 \cdot 3H_2O$ nanosheets, 62.5 mg L^{-1} CuO nanosheets, 62.5 mg L^{-1} CuO commercial nanoparticles, and 125 mg L^{-1} $CuSO_4$ solution were prepared and were sprayed onto the leaves of *A. thaliana* lines. These concentrations were selected based on previous work that demonstrated positive plant response and no overt phytotoxicity.[8,13] Specifically, the solutions were dispersed in a 10 min bath sonicator and ∼3 mL of solution was foliar applied on the leaves of each *A. thaliana* line. The actual Cu concentration across all treatments was equivalent to 50 mg Cu L^{-1}. At 15 min, 2, 4, and 8 h after foliar application, Cu was extracted from three separation fractions as described below: the surface-attached fraction, the cuticle, and the interior leaf tissue. These time points were chosen based on findings from a previous study indicating significant foliar Cu accumulation within the first 8 h.[13] Twelve biological replicates for each mutant were established for each treatment, and one biological replicate that was the source of three leaves for each leaf fraction was used for Cu measurement.

Cu Measurement. Three uniform leaves that had been amended with Cu were collected from each *A. thaliana* seedling at each time point: 15 min, 2, 4, and 8 h after application. The isolation of the surface-attached fraction, cuticle fraction, and leaf tissue fraction was conducted according to Shen et al.[13] Briefly, (1) DI water (10 mL) was used to wash the outer surface of the leaf for 5 min, and the collected rinsate was designated as the surface-attached fraction; (2) those same leaves were then transferred into 35% nitric acid (10 mL) for 15 min, and the collected nitric acid was designated as the cuticle fraction; and (3) the same water rinsed- and cuticle-free leaves were then digested in concentrated acid (5 mL diluted to 25 mL for analysis) to isolate the interior absorbed Cu fraction. The nitric acid digestion method was conducted on an open hot plate;[22] a 5 mL aliquot of concentrated HNO_3 was added to digestion tubes containing 0.50−0.80 g (three leaves) fresh leaves, and then the samples were incubated overnight. The samples were then digested at 115 °C on a hot block for 45 min, followed by dilution to 25 mL with DI water after cooling for Cu determination. Copper from surface-attached and interior tissue fractions were quantified by inductively coupled plasma optical emission spectroscopy (ICP-OES; Thermo Fisher iCAP 6500; Thermo Fisher Scientific, Waltham, MA). Because of lower sample masses, ICP-MS was used to quantify Cu in the cuticle fraction. The nutrient Mg was monitored as a biomarker in the cuticle fraction to ensure minimal whole leaf damage during the cuticle isolation procedure.[13]

Stomata and Cuticle Effects. To further explore the roles of the stomata and cuticle in nanomaterial transfer from the leaf surface through the cuticle and into the leaf interior over time, a stomatal closure assay was conducted employing the foliar application of abscisic acid (ABA).[23] An ABA solution (50 μM ABA) was applied by foliar spraying onto *Arabidopsis* mutant and wild-type plants until the surface was fully visible covered; this was done on two consecutive days prior to nanomaterial and $CuSO_4$ exposure. Then, 114.2 mg L^{-1} $Cu_3(PO_4)_2 \cdot 3H_2O$ nanosheets, 62.5 mg L^{-1} CuO nanosheets, 62.5 mg L^{-1} CuO commercial nanoparticles, and 125 mg L^{-1} $CuSO_4$ solutions were prepared and applied as above. Three uniform leaves were harvested from each *Arabidopsis* mutant at 15 min and 8 h after foliar application; the surface-attached, cuticle, and interior leaf tissue fractions were isolated, and the Cu content was determined as described above.

Leaf Surface Analysis. To characterize the leaf surface of *A. thaliana* stomatal mutants, leaf surface stomata density was investigated by the Axioplan 2 imaging light microscope (CARL ZEISS, Germany) according to Kim et al.[24] To characterize the cuticle of *A. thaliana* cuticle mutants, fully expanded leaves of each mutant were harvested for analysis by attenuated total reflectance−Fourier-transform infrared spectroscopy (ATR-FTIR), with six leaves collected from each line being evaluated. The experiment was performed using a SHIMADZU IRTracer-100 FTIR spectrometer (Shimadzu, Japan) equipped with attenuated total reflectance (ATR) (PIKE Technologies).[25] Univariate statistical analyses were calculated using Spectragry (v1.2.15, Germany).

Statistical Analysis. The elemental content of the three isolated fractions was statistically analyzed using a one-way ANOVA. Twelve individual plants were established for *A. thaliana* mutant lines. For the collection, 12 biological replicates were set in each treatment, and three replicates were set at each time point of the three-leaf fractions (surface-attached, cuticle, leaf tissue); three separate leaves were analyzed for each *A. thaliana* line at each time point. Means were separated using Duncan's significant difference test at $p < 0.05$. All analyses were performed using SPSS 25.0 (IBM).

https://doi.org/10.1021/acs.jafc.1c07873
J. Agric. Food Chem. XXXX, XXX, XXX−XXX

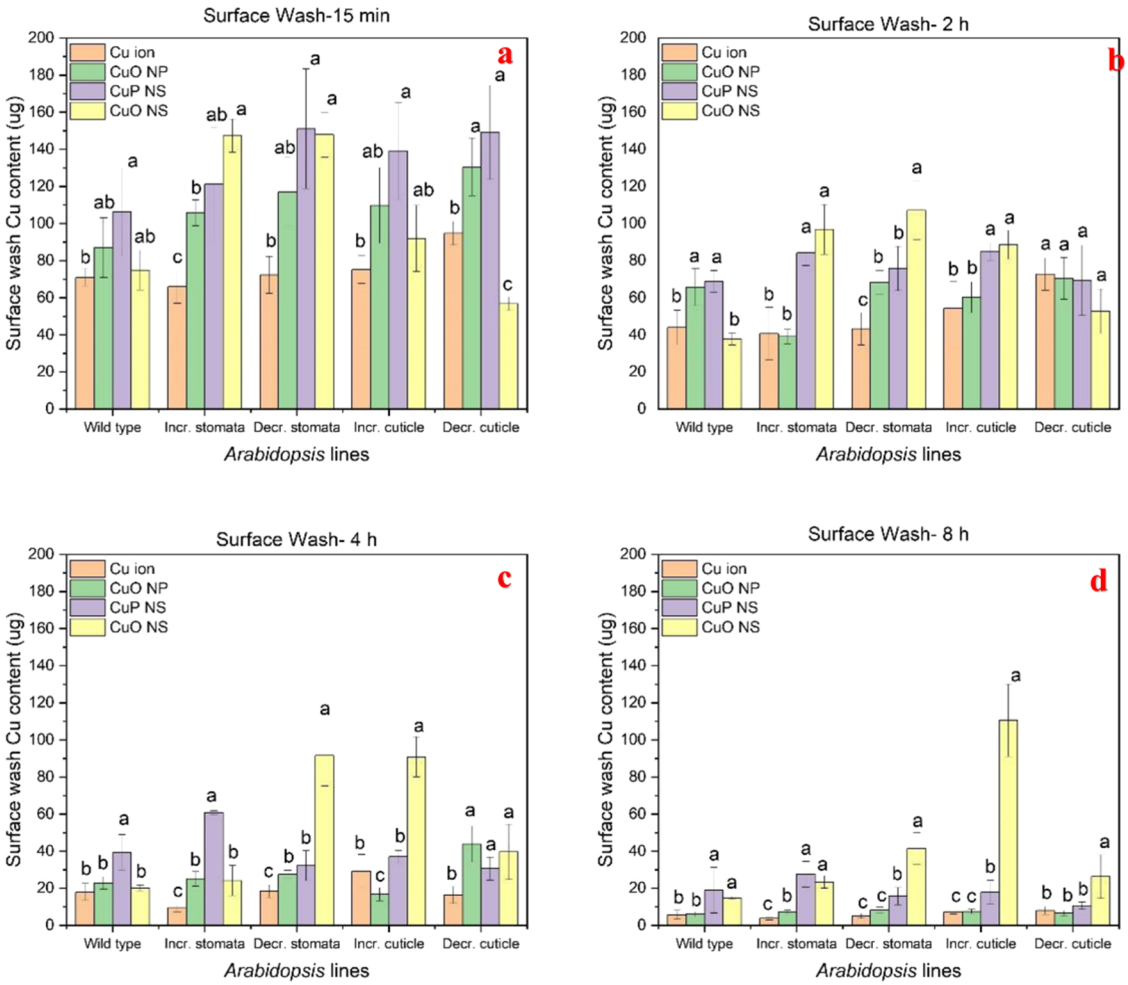

Figure 2. Surface-attached Cu content at 15 min (a), 2 h (b), 4 h (c), and 8 h (d) in *Arabidopsis* wild-type, increased-stomata, decreased-stomata, increased-cuticle, and decreased-cuticle mutants. (Note: within a panel and mutant type, bars with different letters are significantly different; one-way ANOVA with Duncan's test ($p < 0.05$).).

RESULTS

Nanomaterial Characterization and Dissolution. CuO in nanoparticle and nanosheet forms and $Cu_3(PO_4)_3{\cdot}3H_2O$ in nanosheet form were synthesized as described previously.[8] Since CuO and $Cu_3(PO_4)_3{\cdot}3H_2O$ nanomaterials used in the present work are identical to those used previously, we include here only analytical data specific to the batch of nanoparticles used in the present studies.

The ζ-potential values of CuO NP, $Cu_3(PO_4)_2{\cdot}3H_2O$ NS, and CuO NS suspended in deionized water were −11.45, −8.94, and −26.3 mV, respectively (Table S4). The SEM images of these particles are shown in Figure 1a−c and confirm that the morphology of CuO nanosheets were elongated sheets with an average length of 500 ± 200 nm and an average width of 120 ± 40 nm (Figure 1d−f). The nanoparticle powder diffraction pattern was consistent with the monoclinic tenorite crystal structure of CuO. The dissolution of Cu from the different nanomaterials was 0.1−1.4% (Figure S1). $Cu_3(PO_4)_2{\cdot}3H_2O$ NS exhibited the greatest dissolution at 637.30 $\mu g\ L^{-1}$ at 24 h; CuO NPs and CuO NS had different patterns of release and had values of 41.46 and 54.62 $\mu g\ L^{-1}$. These findings align well with previously reported dissolution data for these materials.[11]

Cu Uptake by Wild-Type *A. thaliana*. In wild-type *A. thaliana*, the concentration of Cu in the surface-attached fraction ranged from 70.9 to 106 μg. Specifically, the amount of Cu observed in leaves after exposure to $CuSO_4$ solution, CuO NP, $Cu_3(PO_4)_2{\cdot}3H_2O$ NS, and CuO NS was 70.9, 87.0, 106.2, and 74.8 μg, respectively (Figure 2 and Table S2). These values are not statistically significantly different between the CuO NP, $Cu_3(PO_4)_2{\cdot}3H_2O$ NS, and CuO NS after a 15 min exposure. Over the course of 8 h, the amount of Cu present in the surface-attached fraction steadily declined across all Cu types; notably, these decreases coincided with increases in the cuticle and interior leaf fractions (below). Specifically, for the wild-type, the amount of Cu in the surface-attached fraction with the $CuSO_4$ solution treatment at 2, 4, and 6 h was 44.0, 18.0, and 5.7 μg, respectively; the amounts for the CuO NP were 65.7, 22.8, and 6.1 μg, respectively; the amounts for the $Cu_3(PO_4)_2{\cdot}3H_2O$ NS were 68.8, 39.4, and 19.0 μg, respectively; and the amounts for the CuO NS were 37.6, 20.2, and 14.8 μg, respectively. The amount of Cu in the cuticle fraction at 15 min ranged from 5.31 to 36.3 μg and differed significantly as a function of Cu type (Figure 3 and Table S3). Specifically, the amount in the ionic, CuO NP, $Cu_3(PO_4)_2{\cdot}3H_2O$ NS, and CuO NS was 36.2, 5.3, 8.6, and 22.9 μg, respectively. Over time, the amount of Cu present in the cuticle fraction increased across all Cu types. The amount of

https://doi.org/10.1021/acs.jafc.1c07873
J. Agric. Food Chem. XXXX, XXX, XXX−XXX

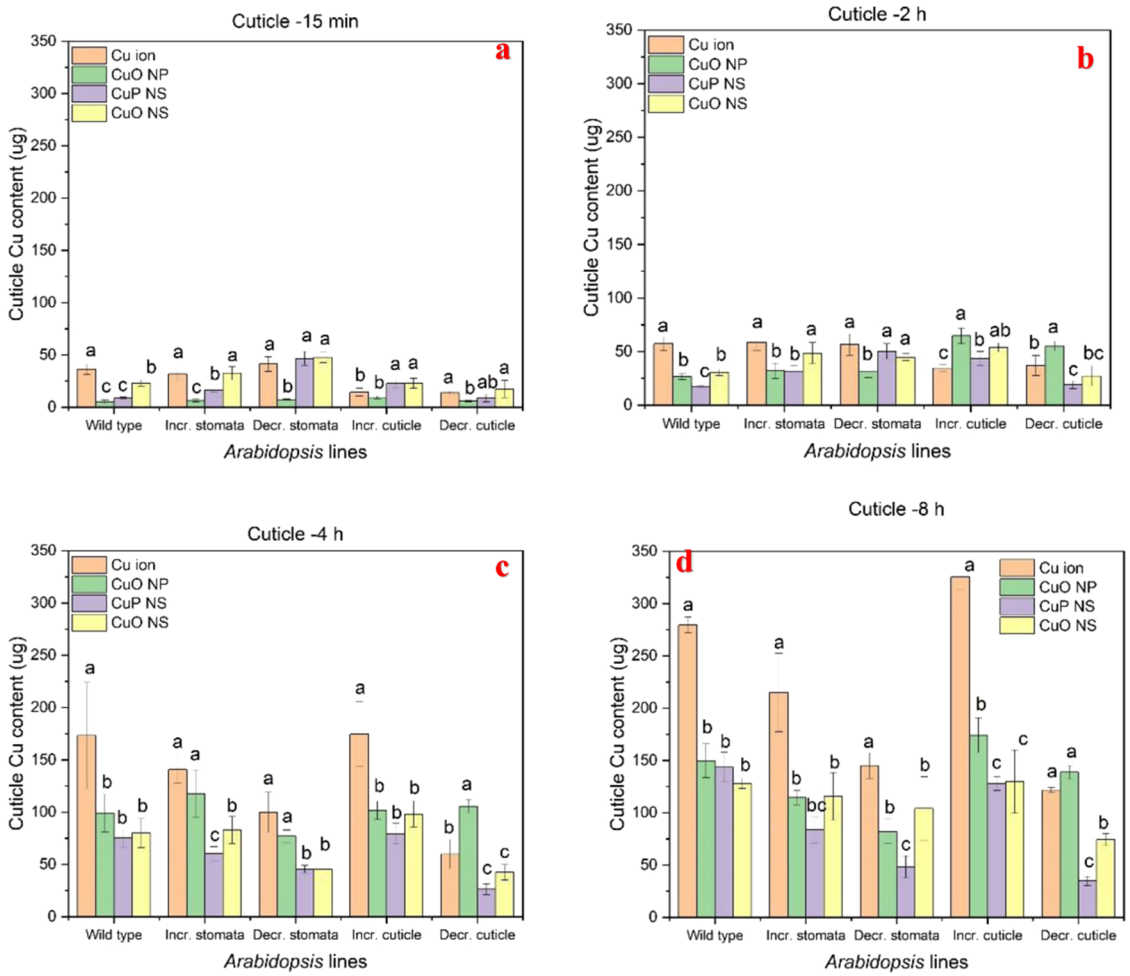

Figure 3. Cuticle Cu content at 15 min (a), 2 h (b), 4 h (c), and 8 h (d) in *Arabidopsis* wild-type, increased-stomata, decreased-stomata, increased-cuticle, and decreased-cuticle mutants. (Note: within a panel and mutant type, bars with different letters are significantly different; one-way ANOVA with Duncan's test ($p < 0.05$).).

Cu in the cuticle fraction with the ionic treatment at 2, 4, and 8 h was 57.3, 173.4, and 279.6 μg, respectively; the amounts for the CuO NP were 26.5, 99.1, 149.7 μg, respectively; the amounts for the $Cu_3(PO_4)_2{\cdot}3H_2O$ NS were 17.0, 75.3, and 143.5 μg, respectively; and the amounts for the CuO NS were 30.7, 79.8, and 128.1 μg, respectively. Interestingly, the amount of Cu retained in the cuticle fraction at 8 h is significantly greater for the ionic treatment than for the three nanoscale forms of Cu. The amount of Cu in the interior leaf fraction at 15 min ranged from 19.3 to 26.8 μg and did not differ as a function of Cu type (Figure 4 and Table S4). The amount of Cu in the interior leaf fraction increased over 8 h for all Cu types. Specifically, the amount of Cu in the interior leaf fraction with the ionic treatment at 2, 4, and 8 h was 57.0, 136.6, and 253.4 μg, respectively; the amounts for the CuO NP were 109.4, 212.6, and 339.5 μg, respectively; the amounts for the $Cu_3(PO_4)_2{\cdot}3H_2O$ NS were 118.2, 188.5, 361.0 μg, respectively; and the amounts for the CuO NS were 111.2, 182.1, 397.4 μg, respectively. Similar to the cuticle fraction, the amount of Cu in the interior leaf fraction for the ionic treatment was significantly different from the nanoscale materials, with the nanomaterials having greater Cu content in the interior leaf fraction. In summary, for wild-type *A. thaliana*, the amount of Cu in the surface-attached fraction steadily declined over 8 h as Cu was transferred to the cuticle and interior leaf tissue fractions and that movement from the surface to the plant was significantly lower for the ionic treatment relative to the nanomaterials.

Cu Uptake by *A. thaliana* Cuticle Mutants. The transfer of Cu from the surface to the interior leaf tissue over 8 h was measured in *A. thaliana* mutants that had either an increased cuticle or possessed a decreased/compromised cuticle. In the increased-cuticle *A. thaliana* mutants, the concentration of Cu in the surface-attached fraction at 15 min ranged from 75.2 to 139.1 μg; for the decreased-cuticle mutants, the range was 56.8−149.2 μg. Specifically, for the increased-cuticle mutants, the amount in the ionic, CuO NP, $Cu_3(PO_4)_2{\cdot}3H_2O$ NS, and CuO NS was 75.1, 109.7, 139.1, and 92.0 μg, respectively (Figure 2); for the decreased-cuticle mutants, these values were 94.8, 130.4, 149.15, and 56.8 μg, respectively. Notably, similar to the wild-type plants, within each mutant type, there were differences as a function of Cu type, with the ionic and CuO NS generally having less Cu in the 15 min surface-attached fraction than the CuO NP and $Cu_3(PO_4)_2{\cdot}3H_2O$ NS treatments. When comparing the "increased" to "decreased" mutant types, the differences appear to be somewhat limited; the Cu contents for CuO NP and $Cu_3(PO_4)_2{\cdot}3H_2O$ NS do not differ significantly based on mutant type. For the ionic treatment, the decreased-cuticle mutants have significantly more Cu in the 15 min surface-attached fraction than do the

https://doi.org/10.1021/acs.jafc.1c07873
J. Agric. Food Chem. XXXX, XXX, XXX−XXX

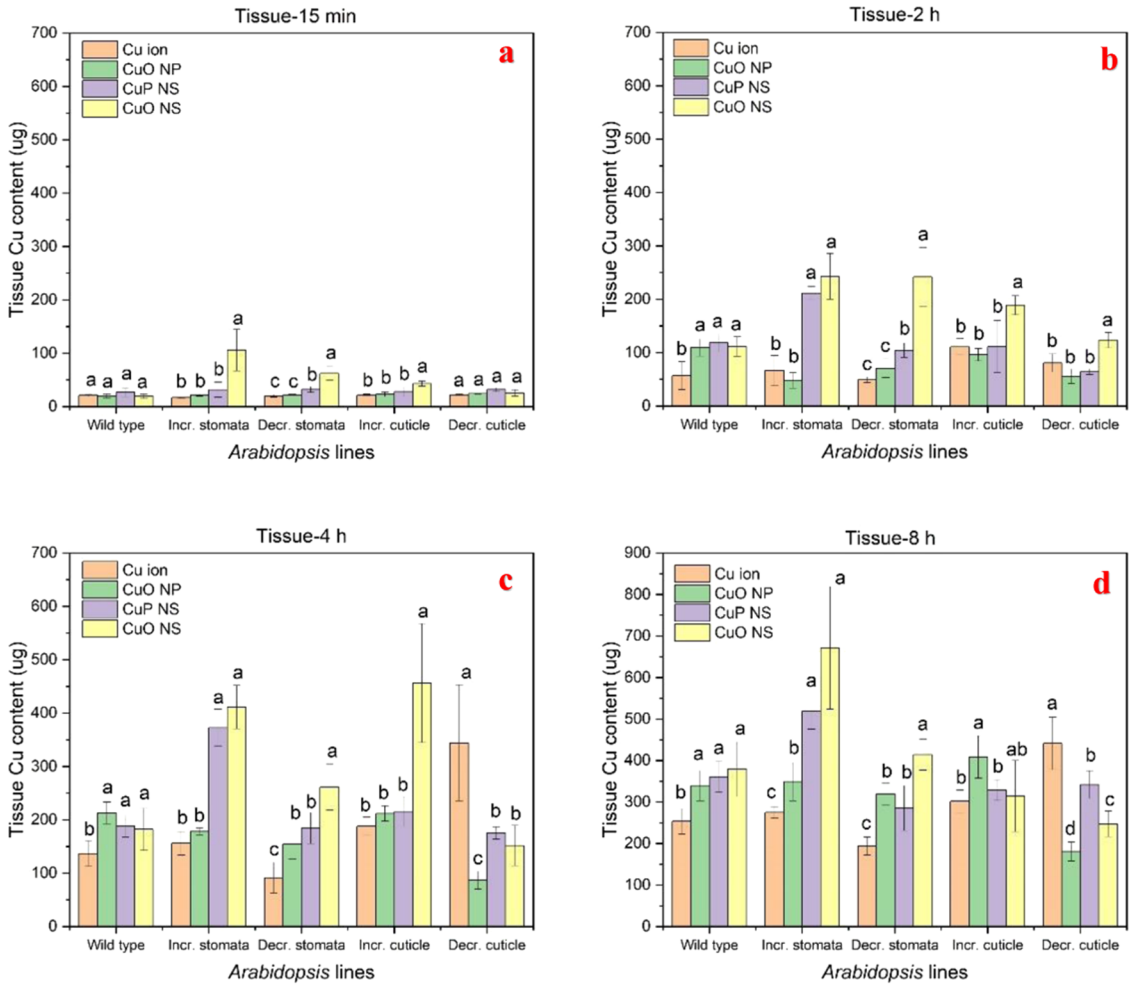

Figure 4. Interior leaf tissue Cu content at 15 min (a), 2 h (b), 4 h (c), and 8 h (d) in *Arabidopsis* wild-type, increased-stomata, decreased-stomata, increased-cuticle, and decreased-cuticle mutants. (Note: within a panel and mutant type, bars with different letters are significantly different; one-way ANOVA with Duncan's test ($p < 0.05$).).

increased-cuticle plants (94.8 μg for the decreased cuticle to 75.2 μg for the increased cuticle); however, the pattern of CuO NS is reversed (56.8–92.0 μg). Across nearly all mutants and Cu types, the amount of Cu in the surface-attached fraction declined over 8 h and did not differ significantly as a function of mutant types, the exception being CuO NS (below). The amount of Cu in the surface-attached fraction of the increased- and decreased-cuticle mutants declined to 7.3 and 7.9 μg, respectively; the amount of Cu for the CuO NP was 7.5 and 6.6 μg (significantly different; $p < 0.05$), respectively; and the amounts for the $Cu_3(PO_4)_2{\cdot}3H_2O$ NS were 18.0 and 10.6 μg, respectively. Conversely, the amount of Cu for the CuO NS in the increased- and decreased-cuticle mutants was 110.5 and 26.3 μg, respectively (significantly different; $p < 0.05$).

The amount of Cu in the cuticle fraction at 15 min ranged from 9.3 to 22.9 μg and 5.9 to 17.4 μg for the increased- and decreased-cuticle mutants, respectively; within both mutant types, the amount of Cu for the CuO NP treatment was significantly less than the other treatments (Figure 3). Across all Cu types and both types of cuticle mutants, the amount of Cu in the cuticle fraction increased significantly over time. At 8 h, the amount of Cu in the cuticle of the increased- and decreased-cuticle mutants increased to 325.5 and 121.7 μg, respectively, for the ionic Cu; the amounts for the CuO NP were 174.1 and 138.6 μg, respectively; the amounts for the $Cu_3(PO_4)_2{\cdot}3H_2O$ NS were 127.9 and 34.9 μg, respectively; and the amounts for the CuO NS were 129.7 and 74.3 μg, respectively. For all Cu types, the decreased-cuticle mutants had significantly less Cu than the increased-cuticle mutants, and the Cu contents are 62.6, 20.0, 73.0, and 42.7% less for ionic Cu, CuO NP, $Cu_3(PO_4)_2{\cdot}3H_2O$ NS, and CuO NS. Although the reasons for the differences as a function of Cu type are unknown, it is not surprising that plants with greater cuticle content would retain larger amounts of analyte in this fraction of the leaf.

The interior leaf tissue Cu content at 15 min ranged from 21.5 to 43.2 and 22.1 to 32.0 μg for the increased- and decreased-cuticle mutants, respectively (Figure 4); there were no statistically significant differences between the mutant types except for CuO NS, where increased- and decreased-cuticle mutants contained 43.2 and 28.2 μg, respectively ($p < 0.05$). Over 8 h, the amount of Cu in the interior leaf tissues increased significantly for all plant and Cu types. At 8 h, the amount of Cu in the interior tissues of the increased- and decreased-cuticle mutants increased to 301.5 and 441.2 μg, respectively, for the ionic treatment; the amounts for the CuO NP were 408.6 and 180.4 μg, respectively; the amounts for the $Cu_3(PO_4)_2{\cdot}3H_2O$ NS were 328.9 and 341.7 μg, respectively; and the amounts for the CuO NS were 314.6 and 247.5 μg, respectively. Notably, for the three nanomaterials, the interior

https://doi.org/10.1021/acs.jafc.1c07873
J. Agric. Food Chem. XXXX, XXX, XXX−XXX

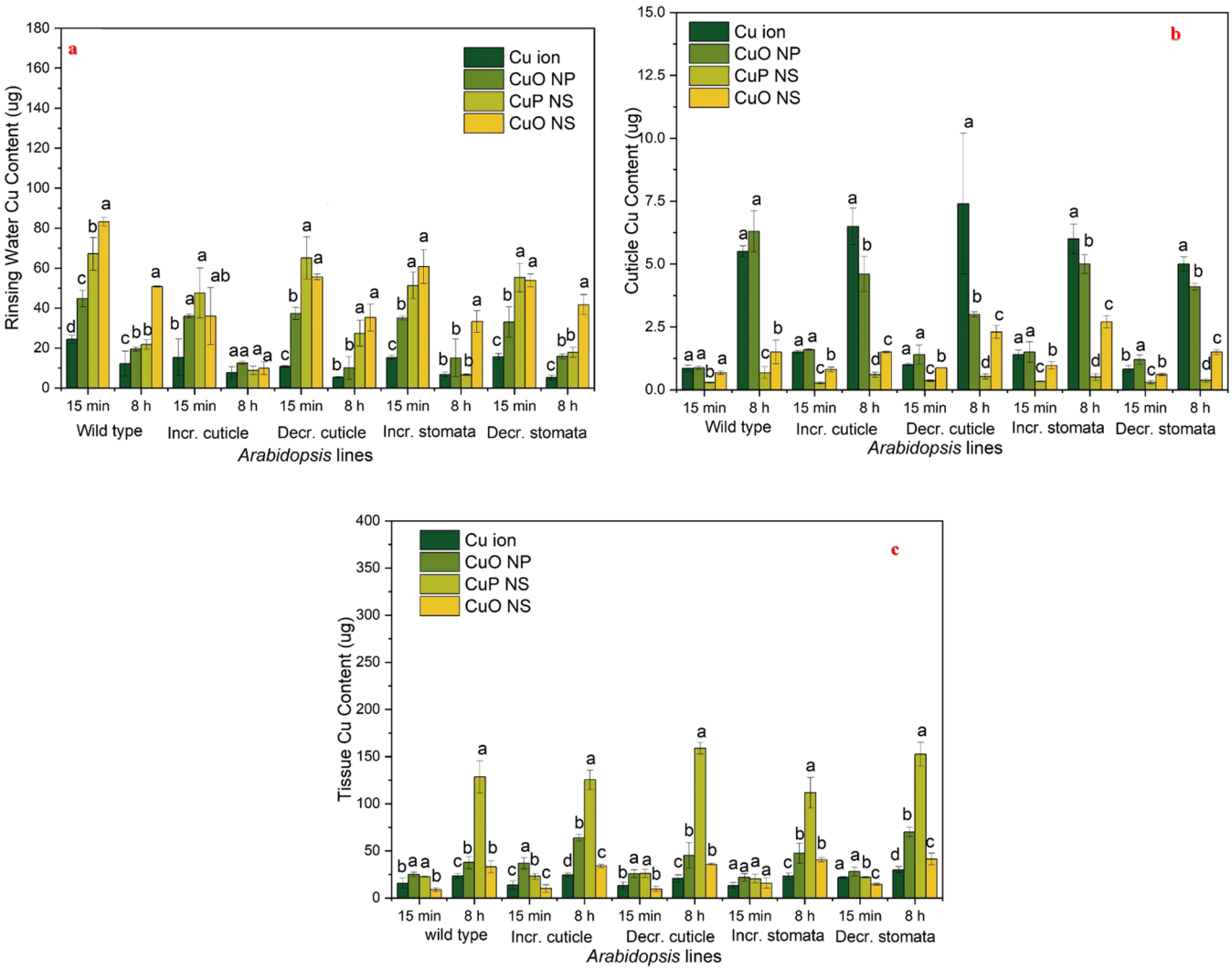

Figure 5. Cu content in surface-attached (a), cuticle (b), and leaf tissue (c) at 15 min and 8 h in *Arabidopsis* wild-type, increased-stomata, decreased-stomata, increased-cuticle, and decreased-cuticle mutants after ABA foliar application. (Note: within a mutant type and time point, bars with different letters are significantly different; one-way ANOVA with Duncan's test ($p < 0.05$).).

leaf tissues of the increased-cuticle mutants had either statistically equivalent or greater Cu content than the decreased-cuticle mutants. This is an important finding because if the cuticle pathway was a significant route of entry for Cu nanomaterials or Cu derived from nanomaterials (ionic Cu), one would expect the opposite finding; a decreased or compromised cuticle would yield greater leaf Cu content. Interestingly, that is precisely the finding for the ionic Cu treatment, the Cu content in the decreased-cuticle mutants is 46% greater than in the increased-cuticle mutants in the interior tissues. These findings clearly imply nanoscale-specific processes of attachment, accumulation, and/or dissolution at the leaf biointerface.

Cu Uptake by *A. thaliana* Stomatal Mutants. The time-dependent movement of Cu from the surface to the interior leaf tissue was measured in *A. thaliana* mutants that had either increased- or decreased-stomatal density. In the increased-stomata density *A. thaliana* mutants, the concentration of Cu in the surface-attached fraction at 15 min ranged from 66.0 to 147.3 μg; for the decreased-cuticle mutants, the range was 72.3−151.0 μg. Specifically, for the increased-stomata mutants, the amount at 15 min in the $CuSO_4$, CuO NP, $Cu_3(PO_4)_2 \cdot 3H_2O$ NS, and CuO NS treatment was 66.0, 105.7, 121.2, and 147.3 μg, respectively (Figure 2); for the decreased-stomata mutants, these values were 72.3, 117.0, 151.0, and 147.9 μg, respectively. Notably, similar to the wild-type and cuticle mutant plants, within each mutant type, there were differences as a function of Cu source, with the ionic treatment having significantly less Cu in the 15 min surface-attached fraction than the nanomaterial treatments. When directly comparing the increased to decreased mutant types, there were no differences of statistical significance at 15 min in the surface-attached fraction. Across all mutant and Cu types, the amount of Cu in the surface-attached fraction declined over 8 h and did not differ significantly as a function of mutant type; Cu contents for the ionic and CuO NP treatments did differ significantly for the two nanosheets in the surface-attached fraction. The amount of Cu in the surface-attached fraction of the increased- and decreased-stomata mutants declined to 3.8 and 5.1 μg, respectively, for the ionic treatment; the amounts for the CuO NP were 7.4 and 8.2 μg, respectively; the amount for the $Cu_3(PO_4)_2 \cdot 3H_2O$ NS was 27.6 and 15.8 μg, respectively ($p < 0.05$); and the amounts for the CuO NS were 23.4 and 41.5 μg, respectively ($p < 0.05$).

https://doi.org/10.1021/acs.jafc.1c07873
J. Agric. Food Chem. XXXX, XXX, XXX−XXX

The amount of Cu in the cuticle fraction at 15 min ranged from 6.4 to 32.6 and 7.4 to 47.6 μg for the increased- and decreased-stomata mutants, respectively; similar to the *A. thaliana* cuticle mutants, within both stomata mutant types, the amount of Cu for the CuO NP treatment was significantly less than the other treatments (Figure 3a and Table S4). Across all Cu types and both types of stomata mutants, the amount of Cu in the cuticle fraction increased significantly over time. Specifically, at 8 h the amount of Cu in the cuticle of the increased- and decreased-stomata mutants increased to 215.0 and 145.1 μg, respectively, for the ionic Cu; the amounts for the CuO NP were 114.3 and 82.1 μg, respectively; the amounts for the $Cu_3(PO_4)_2{\cdot}3H_2O$ NS were 83.7 and 48.13 μg, respectively; the amounts for the CuO NS were 115.5 and 104.2 μg. For ionic, CuO NP, and $Cu_3(PO_4)_2{\cdot}3H_2O$ NS, the increased-stomata mutants had significantly more Cu in the cuticle than the decreased-stomata mutants: 48.1, 39.3, and 73.9% more for ionic Cu, CuO NP, and $Cu_3(PO_4)_2{\cdot}3H_2O$ NS, respectively. It is not surprising that plants with greater stomatal density would accumulate larger amounts of the analyte.

The interior leaf tissue Cu content at 15 min ranged from 17.1 to 105.9 and 19.9 to 62.3 μg for the increased-and decreased-stomata mutants, respectively (Figure 4). There were no statistically significant differences between the mutant types except for CuO NS, where increased and decreased mutants contained 105.6 and 62.3 μg, respectively (significantly different; $p < 0.05$). The significantly greater accumulation of Cu from the CuO nanosheets in the increased-stomatal mutants is notable relative to all other treatments and *A. thaliana* plants, including wild type. At 8 h, the amount of Cu in the interior tissues of the increased- and decreased-cuticle mutants increased to 274.7 and 194.1 μg, respectively, for the ionic treatment; the amount for the CuO NP was 349.0 and 319.5 μg, respectively; the amount for the $Cu_3(PO_4)_2{\cdot}3H_2O$ NS was 518.4 and 285.1 μg, respectively; the amount for the CuO NS was 671.3 and 414.2 μg, respectively. Notably, for all Cu types, the interior leaf tissue of the increased-stomata mutants had greater Cu content than those of the decreased-stomata mutants. This is an important finding because if the stomatal pathway is a significant route of entry for Cu nanomaterials or Cu derived from nanomaterials, one would expect this exact result. To get a final assessment of Cu content at 8 h, the amount of Cu in the surface-attached, cuticle, and interior leaf fractions at the final time point were summed and compared across stomata mutant type. For the decreased-stomata mutants, the total Cu content of the three fractions at 8 h was 344.3, 409.8, 349.0, and 559.8 μg for the ionic, CuO NP, $Cu_3(PO_4)_2{\cdot}3H_2O$ NS, and CuO NS treatments, respectively; in comparison, the values for the increased-stomata mutants were 492.8, 470.7, 629.7, and 810.2 μg, respectively. The increased-stomata mutant Cu content is 1.43-, 1.15-, 1.80-, and 1.45-fold greater for the ionic, CuO NP, $Cu_3(PO_4)_2{\cdot}3H_2O$ NS, and CuO NS treatments than present in the decreased-stomata mutants. These findings clearly highlight the stomatal pathway as the dominant route of Cu entry, regardless of Cu type.

ABA-Induced Stomatal Closure Assay. As noted above, ABA is a plant hormone which is associated endogenously with stomatal closure and has been used as an exogenous amendment to induce the closing of these pores and to study subsequent physiological impacts on plants.[23] Based on the above findings highlighting the critical role of the stomatal pathway in the intraleaf accumulation of Cu in both ionic and nanoscale forms, we exogenously applied ABA to the *A. thaliana* wild-type and mutant leaves and determined the Cu content from ionic and nanoscale foliar amendments in the surface-attached, cuticle, and interior leaf tissues at 15 min and 8 h (Figure 5). After 8 h exposure, the content of Cu in the interior leaf tissue was 112.4−145.1 μg and did not differ significantly as a function of *A. thaliana* mutant type. Notably, regardless of Cu or mutant type, these values are all significantly lower than the non-ABA experiments noted above, where 8 h interior tissue Cu content ranged from 180.4 to 414.2 μg. More importantly, the increased accumulation of Cu noted above in interior leaf tissue for all Cu types in the increased-stomata mutants over the decreased-stomata mutants had completely disappeared with ABA treatment. The contents of Cu in the interior leaf tissue at 8 h for the increased and decreased ABA-treated stomata mutants for ionic, CuO NP, $Cu_3(PO_4)_2{\cdot}3H_2O$ NS, and CuO NS treatments were 26.7 and 33.5 μg, 46.9 and 60.31 μg, 112.4 and 134.0 μg, and 42.5 and 34.6 μg, respectively. This adds further certainty to the more important role of the stomatal pathway for the uptake of Cu derived from foliar applied ionic and Cu nanomaterials relative to the cuticle. Interestingly, there are significant differences in the 8 h interior tissue content as a function of Cu types and these differences do not necessarily coincide with data from the non-ABA-treated plants. For example, with ABA treatment, the Cu content from the $Cu_3(PO_4)_2{\cdot}3H_2O$ NS treatment ranged from 112.4 to 145.1 μg and was consistently significantly ($p < 0.05$) greater than the other Cu sources, regardless of mutant types (17.1−64.0 μg). In the non-ABA-treated plants, there were no instances where the $Cu_3(PO_4)_2{\cdot}3H_2O$ NS treatment gave rise to the greater 8 h interior leaf tissue content.

DISCUSSION

Nanomaterial Chemistry and Cuticular Pathway. As noted above, there are two main pathways of nanomaterial transfer from the leaf surface to the interior leaf tissue: the cuticle and the stomata.[20,26] The cuticle makes up the vast majority of the leaf surface and is composed of a hydrophobic and insoluble barrier permeated with soluble waxes.[27] Vráblová et al. reported that the major organic constituents of the *Arabidopsis* leaf cuticle included palmitic acids (1.44 mg cm^{-2}), stearic acids (0.32 mg cm^{-2}), hentriacontane (0.45 mg cm^{-2}), octacosanol (0.11 mg cm^{-2}), nonacosane (0.27 mg cm^{-2}), and hexacosanol (0.07 mg cm^{-2}).[14] Nanoparticle transfer through this surface chemistry of macromolecular organic acids and long-chain alkanes could be difficult and hetero- and homoaggregation to larger particles may be strongly favored.[28] For example, paraffin has been used as an agent in which to store Fe_3O_4 nanoparticles, and palmitic acid has been applied as a cap and reducer agent for Fe_3O_4 nanoparticles.[29] Similarly, Choudhuri and Datta reported that a two-dimensional network of thiol-capped Au nanoparticle clusters self-organized on a stearic acid monolayer on water; the nanoparticles were unable to penetrate the tension formed at the stearic acid and water interface.[30] This level of nanoparticle−organic constituent interaction seems to suggest that most nanomaterials would have difficulty in traversing the complex organic barrier provided by the cuticle.

Importantly, the cuticle is the outer layer, but to a certain extent, it does form a continuum with the polysaccharide-dominated plant cell wall (30−50% cellulose, 20−35% xylem,

https://doi.org/10.1021/acs.jafc.1c07873
J. Agric. Food Chem. XXXX, XXX, XXX−XXX

and 10−25% lignin); these components are chemically quite different from that of the cuticle.[31] The cuticle and plant leaf surface, in general, exhibit weak positive field intensities at 100−400 V cm^{-1}, and this overall positive charge will electrostatically attract negatively charged particles on the surface.[32,33] The ζ-potential of the materials used in the current study is shown in Table S5. All nanomaterials used here present a negative ζ-potential (−26.3 to −8.94 mV), which would indicate favorable electrostatic interactions with the cuticle surface. This weak electrostatic surface interaction explains why the surface-attached fraction of all of the materials from the leaf surface was initially high at 15 min (Figure 2). Importantly, this pattern was exhibited by the wild-type *A. thaliana*, with the surface-attached fraction at 15 min containing the greatest amount of Cu from $Cu_3(PO_4)_2{\cdot}3H_2O$ nanosheets and the least from CuO nanosheets. In solution, Cu from $CuSO_4$ will exhibit a positive charge,[34] leading to weak electrostatic repulsion from the cuticular surface. Additionally, Cu^{2+} may bind electrostatically to any negatively charged macromolecular organic acids with proton-binding characteristics within the cuticle, such as humic and fulvic (hydrophobic) acids.[35] Given this, the observed accumulation of Cu from the ionic treatment in the cuticle fraction is not surprising (Figure 3).

In our study, FTIR analysis of *A. thaliana* mutants revealed that the increased-cuticle mutants have greater amounts of C═C bonds, aldehyde groups, and carbonyl groups relative to the decreased-cuticle mutants and wild-type controls (Figure S2 and Table S2). Importantly, although these rather significant changes in cuticle chemistry and overall amount did result in greater Cu retention within the cuticle, there was no impact on the transfer of Cu derived from Cu nanomaterials through the cuticle and into the leaf interior. Epicuticular waxes are deposited on the outer surface as a more or less uniform and amorphous layer or in the form of discontinuous agglomerations. The cuticle matrix underneath is chiefly composed (40−80% weight) of cutin, a polymer with a network of oxygenated C16 and/or C18 fatty acids cross-linked by ester bonds. Depending on the species, the quantity of cutin controls the thickness, and the numbers of ethylene linkages, aldehyde groups, and carbonyl groups can mediate the quantity of cutin. Based on the FTIR results, the number of ethylene linkages of the increased-cuticle mutants is significantly greater ($p < 0.05$) than that in the wild-type and the decreased-cuticle mutants (Table S2), indicating greater thickness in the increased-cuticle mutants.

Importantly, in addition to charge, Cu movement from the surface to the leaf will also be impacted by particle morphology and dissolution.[36,37] In solution, the measured nanomaterial hydrodynamic size was as follows: $Cu_3(PO_4)_2{\cdot}3H_2O$ nanosheets (1079 nm) > CuO commercial nanoparticles (628 nm) > CuO nanosheets (319 nm) (Table S5). However, these measurements may have little relevance to Cu nanomaterial fate and transformation on the leaf surface over the course of 8 h. The dissolution rates of $Cu_3(PO_4)_2{\cdot}3H_2O$ NS, CuO NPs, and CuO NS were 240.16, 27.49, and 76.73 μg L^{-1} at 8 h, respectively. These data align with the experimental and computational dissolution results of the same materials in Ma et al.,[11] both in terms of the absolute amount of Cu release from each material type and the relative amounts across the materials. For the wild-type *A. thaliana*, although there were some differences in the amount of Cu from the different nanomaterials in the different leaf fractions from 15 min to 4 h, the amount in the interior leaf tissue at 8 h did not vary significantly as a function of Cu type. A larger number of statistically significant differences in Cu content were noted in the various *A. thaliana* mutants, but the role of mutant type complicates correlating Cu accumulation with dissolution profile. In addition, given the low overall dissolution rate (less than 1.5%) and a large number of differences between solution-based measurements and the leaf surface, the relationship between dissolution and Cu movement through the leaf fractions over an 8 h period may be tenuous at best.

Nanomaterial Composition and Stomatal Pathway. As noted above, the stomatal pathway plays a dominant role in the accumulation of Cu from the nanomaterial and ionic foliar amendments in both wild type and mutant *A. thaliana*. The summed Cu content of the surface-attached, cuticle, and interior tissue fractions for the increased-stomata mutants was 1.15−1.80 times greater than that of the decreased-stomata plants. Not surprisingly, this data correlated with the observed stomatal density on the leaf surfaces; the increased-stomata mutant, decreased-stomata mutant, and wild-type leaves possessed 134.68, 94.70, and 113.64 stomata/mm^2, respectively (Figure S3 and Table S3). In addition, foliar pretreatment with ABA to close the stomata reduced Cu content in all mutants across all Cu nanomaterial types and eliminated the differences between the increased- and decreased-stomatal mutants. This data clearly implicates the stomatal pathway as the dominant entry point for Cu derived from Cu nanomaterials and salt forms. This data aligns well with the previous results demonstrating that the stomata are key to the internationalization of Ag NPs in plant leaves.[38] Similarly, upon foliar application of Ag NPs and $AgNO_3$, SEM-EDS showed that Ag NPs were found in the *Lactuca sativa* leaf stomata, whereas Ag ions were dispersed across the leaf surface.[39] Xiong et al. also reported that on lettuce leaf surfaces, SEM-EDS observation revealed that the majority of CuO NPs were detected in the stomata while the Cu ions were more scattered on the leaf surface.[40] Zhu et al. foliar applied fluorescein isothiocyanate (FITC)-tagged ZnO NPs to wheat leaves and used confocal microscopy to show that these materials appeared to move through the stomata to the apoplast prior to transport into the leaf mesophyll. Importantly, the reduced stomatal aperture was directly associated with decreased Zn content in the leaf apoplast and cytoplasm.[41] These findings align well with the results from our study. Also, stomatal closure was observed during CuO NPs−leaf contact on water hyacinth leaf surfaces,[42] and the data clearly suggested that the more open structure of the stomata, the greater nanomaterial passage into the interior leaf.[43,44] Interestingly, while foliar fertilization with salt or ionic forms of micronutrients has been successfully used to improve plant nutrition in agriculture,[45,46] our results and that of the supporting literature clearly demonstrate that the cuticle serves as an effective barrier for amendments in this form. Nanoscale amendments with strategies that specifically target stomatal and guard cell attachment may prove far more effective at foliar feeding for both crop nutrition and disease resistance.[47]

The plant leaf cuticle is among the most significant environmental biointerfaces serving as a hydrophobic boundary between the outer environment and interior plant tissues. The current study demonstrates that the cuticular pathway is not particularly important for Cu nanomaterial uptake, as Cu tissue concentrations for increased-cuticle and decreased-cuticle mutants did not differ. Conversely, the Cu leaf tissue

https://doi.org/10.1021/acs.jafc.1c07873
J. Agric. Food Chem. XXXX, XXX, XXX−XXX

content of *A. thaliana* increased-stomatal mutants was significantly greater than that of the decreased stomatal mutants across all Cu types. In addition, exogenous treatment with ABA to close the stomata reduced Cu content in all mutants across all Cu types and eliminated the differences between the increased- and decreased-stomatal mutants. These findings clearly highlight the significance of the stomatal uptake pathway for nanomaterial foliar accumulation. Additional study should focus on determining the precise form of Cu as the element moves through the cuticle and into the leaf and, importantly, correlate that process with initial nanomaterial properties such as composition, morphology, and dissolution profile. These findings increase our understanding of nanomaterial chemical interactions at the leaf biointerface and directly inform nanomaterial synthesis so as to optimize this functionality for strategies of nutrient amendment in sustainable nanoenabled agriculture.

■ ASSOCIATED CONTENT

Supporting Information

The Supporting Information is available free of charge at https://pubs.acs.org/doi/10.1021/acs.jafc.1c07873.

Section S1: nanomaterial characterization; Section S2: *Arabidopsis* mutant properties; Section S3: raw data of the surface-attached, cuticle, and tissue fractions; Section S4: ζ-potential and particle size of the nanomaterials in deionized water; Section S5: individual cuticle and stomata mutants' response to Cu nanomaterials; Section S6: three-factor analysis of cuticle and stomata variance (PDF)

■ AUTHOR INFORMATION

Corresponding Authors

Robert J. Hamers − *The NSF Center for Sustainable Nanotechnology, Department of Chemistry, University of Wisconsin−Madison, Madison, Wisconsin 53706, United States*; orcid.org/0000-0003-3821-9625; Email: rjhamers@wisc.edu

Jason C. White − *The NSF Center for Sustainable Nanotechnology, Department of Analytical Chemistry, The Connecticut Agricultural Experiment Station, New Haven, Connecticut 06504, United States*; orcid.org/0000-0001-5001-8143; Email: Jason.White@ct.gov

Authors

Yu Shen − *The NSF Center for Sustainable Nanotechnology, Department of Chemistry, University of Wisconsin−Madison, Madison, Wisconsin 53706, United States*

Jaya Borgatta − *The NSF Center for Sustainable Nanotechnology, Department of Chemistry, University of Wisconsin−Madison, Madison, Wisconsin 53706, United States*

Chuanxin Ma − *The NSF Center for Sustainable Nanotechnology, Department of Analytical Chemistry, The Connecticut Agricultural Experiment Station, New Haven, Connecticut 06504, United States*; orcid.org/0000-0001-5125-7322

Gurpal Singh − *Stockbridge School of Agriculture, University of Massachusetts Amherst, Amherst, Massachusetts 01003, United States*

Carlos Tamez − *The NSF Center for Sustainable Nanotechnology, Department of Chemistry, University of Wisconsin−Madison, Madison, Wisconsin 53706, United States*

Neil P. Schultes − *The NSF Center for Sustainable Nanotechnology, Department of Plant Pathology and Ecology, The Connecticut Agricultural Experiment Station, New Haven, Connecticut 06504, United States*

Zhiyun Zhang − *Department of Food Science, University of Massachusetts Amherst, Amherst, Massachusetts 01003, United States*

Om Parkash Dhankher − *Stockbridge School of Agriculture, University of Massachusetts Amherst, Amherst, Massachusetts 01003, United States*; orcid.org/0000-0003-0737-6783

Wade H. Elmer − *The NSF Center for Sustainable Nanotechnology, Department of Plant Pathology and Ecology, The Connecticut Agricultural Experiment Station, New Haven, Connecticut 06504, United States*; orcid.org/0000-0003-3308-4899

Lili He − *Department of Food Science, University of Massachusetts Amherst, Amherst, Massachusetts 01003, United States*

Complete contact information is available at: https://pubs.acs.org/10.1021/acs.jafc.1c07873

Author Contributions

Y.S., G.S., Z.Z., and C.T. performed the experiment; J.B. synthesized the nanoparticles and performed nanomaterial characterization; W.H.E., J.C.W., and R.J.H. designed the experiment; Y.S., C.M., and J.C.W. carried out the data analysis and Y.S. did the graphics designs; Y.S. drafted the manuscript, and O.P.D., W.H.E., L.H., R.J.H., and J.C.W. reviewed and edited the manuscript.

Notes

The authors declare no competing financial interest.

■ ACKNOWLEDGMENTS

This material is based upon work supported by the National Science Foundation under Grant No. CHE-2001611, the NSF Center for Sustainable Nanotechnology (CSN). The CSN is part of the Centers for Chemical Innovation Program. In this study, Craig Musante supported the ICP-MS work; and Dr. Marie Hronková shared information on plant cuticle chemical composition.

■ ABBREVIATIONS

NS, nanosheets; NPs, nanoparticles; NM, nanomaterials

■ REFERENCES

(1) Handford, C. E.; Dean, M.; Henchion, M.; Spence, M.; Elliott, C. T.; Campbell, K. Implications of nanotechnology for the agri-food industry: Opportunities, benefits and risks. *Trends Food Sci. Technol.* **2014**, *40*, 226−241.

(2) Shen, Y.; Tang, H.; Wu, W.; Shang, H.; Zhang, D.; Zhan, X.; Xing, B. Role of nano-biochar in attenuating the allelopathic effect from Imperata cylindrica on rice seedlings. *Environ. Sci.: Nano* **2020**, *7*, 116−126.

(3) Dimkpa, C. O.; Andrews, J.; Sanabria, J.; Bindraban, P. S.; Singh, U.; Elmer, W. H.; Gardea-Torresdey, J. L.; White, J. C. Interactive effects of drought, organic fertilizer, and zinc oxide nanoscale and bulk particles on wheat performance and grain nutrient accumulation. *Sci. Total. Environ.* **2020**, *722*, No. 137808.

(4) An, J.; Hu, P.; Li, F.; Wu, H.; Shen, Y.; White, J. C.; Tian, X.; Li, Z.; Giraldo, J. P. Emerging investigator series: molecular mechanisms

of plant salinity stress tolerance improvement by seed priming with cerium oxide nanoparticles. *Environ. Sci.: Nano* **2020**, *7*, 2214−2228.

(5) Wang, A.; Jin, Q.; Xu, X.; Miao, A.; White, J. C.; Gardea-Torresdey, J. L.; Ji, R.; Zhao, L. High-throughput screening for engineered nanoparticles that enhance photosynthesis using mesophyll protoplasts. *J. Agric. Food Chem.* **2020**, *68*, 3382−3389.

(6) Nandhini, M.; Rajini, S. B.; Udayashankar, A. C.; Niranjana, S. R.; Lund, O. S.; Shetty, H. S.; Prakash, H. S. Biofabricated zinc oxide nanoparticles as an eco-friendly alternative for growth promotion and management of downy mildew of pearl millet. *Crop Prot.* **2019**, *121*, 103−112.

(7) Buchman, J. T.; Elmer, W. H.; Ma, C.; Landy, K. M.; White, J. C.; Haynes, C. L. Chitosan-Coated Mesoporous Silica Nanoparticle Treatment of Citrullus lanatus (Watermelon): Enhanced Fungal Disease Suppression and Modulated Expression of Stress-Related Genes. *ACS Sustainable Chem. Eng.* **2019**, *7*, 19649−19659.

(8) Borgatta, J.; Ma, C.; Hudson-Smith, N.; Elmer, W.; Plaza Pérez, C. D.; De La Torre-Roche, R.; Zuverza-Mena, N.; Haynes, C. L.; White, J. C.; Hamers, R. J. Copper based nanomaterials suppress root fungal disease in watermelon (*Citrullus lanatus*): Role of particle morphology, composition and dissolution behavior. *ACS Sustainable Chem. Eng.* **2018**, *6*, 14847−14856.

(9) Ma, C.; Borgatta, J.; De La Torre-Roche, R.; Zuverza-Mena, N.; White, J. C.; Hamers, R. J.; Elmer, W. H. Time-dependent transcriptional response of tomato (*Solanum lycopersicum* L.) to Cu nanoparticle exposure upon infection with *Fusarium oxysporum* f. sp. lycopersici. *ACS Sustainable Chem. Eng.* **2019**, *7*, 10064−10074.

(10) Xu, T.; Ma, C.; Aytac, Z.; Hu, X.; Ng, K. W.; White, J. C.; Demokritou, P. Enhancing agrichemical delivery and seedling development with biodegradable, tunable, biopolymer-based nanofiber seed coatings. *ACS Sustainable Chem. Eng.* **2020**, *8*, 9537−9548.

(11) Ma, C.; Borgatta, J.; Hudson, B. G.; Tamijani, A. A.; De La Torre-Roche, R.; Zuverza-Mena, N.; Shen, Y.; Elmer, W.; Xing, B.; Mason, S. E.; Hamers, R. J.; White, J. C. Advanced material modulation of nutritional and phytohormone status alleviates damage from soybean sudden death syndrome. *Nat. Nanotechnol.* **2020**, *15*, 1033−1042.

(12) Elmer, W. H.; White, J. C. The use of metallic oxide nanoparticles to enhance growth of tomatoes and eggplants in disease infested soil or soilless medium. *Environ. Sci.: Nano* **2016**, *3*, 1072−1079.

(13) Shen, Y.; Borgatta, J.; Ma, C.; Elmer, W.; Hamers, R. J.; White, J. C. Copper nanomaterial morphology and composition control foliar transfer through the cuticle and mediate resistance to root fungal disease in tomato (*Solanum lycopersicum*). *J. Agric. Food Chem.* **2020**, *68*, 11327−11338.

(14) Vráblová, M.; Vrabl, D.; Sokolova, B.; Markova, D.; Hronkova, M. A modified method for enzymatic isolation of and subsequent wax extraction from *Arabidopsis thaliana* leaf cuticle. *Plant Methods* **2020**, *16*, No. 129.

(15) Page, A. P.; Johnstone, I. L. The cuticle. *WormBook* **2007**, 1−15.

(16) Dietrich, P.; Sanders, D.; Hedrich, R. The role of ion channels in light-dependent stomatal opening. *J. Exp. Bot.* **2001**, *52*, 1959−1967.

(17) Kranjc, E.; Mazej, D.; Regvar, M.; Drobne, D.; Remškar, M. Foliar surface free energy affects platinum nanoparticle adhesion, uptake, and translocation from leaves to roots in arugula and escarole. *Environ. Sci.: Nano* **2018**, *5*, 520−532.

(18) Eichert, T.; Goldbach, H. E. Equivalent pore radii of hydrophilic foliar uptake routes in stomatous and astomatous leaf surfaces-further evidence for a stomatal pathway. *Physiol. Plant* **2008**, *132*, 491−502.

(19) Wang, W. N.; Tarafdar, J. C.; Biswas, P. Nanoparticle synthesis and delivery by an aerosol route for watermelon plant foliar uptake. *J. Nanopart. Res.* **2013**, *15*, No. 1417.

(20) Avellan, A.; Yun, J.; Zhang, Y.; Spielman-Sun, E.; Unrine, J. M.; Thieme, J.; Li, J.; Lombi, E.; Bland, G.; Lowry, G. V. Nanoparticle size and coating chemistry control foliar uptake pathways, translocation, and leaf-to-rhizosphere transport in wheat. *ACS Nano* **2019**, *13*, 5291−5305.

(21) Hu, P.; An, J.; Faulkner, M. M.; Wu, H.; Li, Z.; Tian, X.; Giraldo, J. P. Nanoparticle charge and size control foliar delivery efficiency to plant cells and organelles. *ACS Nano* **2020**, *14*, 7970−7986.

(22) Shen, Y.; Chen, Q.; Zhang, K.; Zhou, X.; Fang, Y.; Zhan, X. Novel assessment indexes on heavy metal pollution in the environment: Extracellular segregation coefficient and segregation coefficient of intercellular organelles. *Fresenius Environ. Bull.* **2019**, *28*, 5405−5414.

(23) van Iersel, M. W.; Seader, K.; Dove, S. Exogenous abscisic acid application effects on stomatal closure, water use, and shelf life of hydrangea (*Hydrangea macrophylla*). *J. Environ. Hortic.* **2009**, *27*, 234−238.

(24) Kim, J. H.; Oh, Y.; Yoon, H.; Hwang, I.; Chang, Y. S. Iron nanoparticle-induced activation of plasma membrane H^+-ATPase promotes stomatal opening in *Arabidopsis thaliana*. *Environ. Sci. Technol.* **2015**, *49*, 1113−1119.

(25) Liu, N.; Zhao, L.; Tang, L.; Stobbs, J.; Parkin, I.; Kunst, L.; Karunakaran, C. Mid-infrared spectroscopy is a fast screening method for selecting Arabidopsis genotypes with altered leaf cuticular wax. *Plant Cell Environ.* **2020**, *43*, 662−674.

(26) Spielman-Sun, E.; Avellan, A.; Bland, G. D.; Clement, E. T.; Tappero, R. V.; Acerbo, A. S.; Lowry, G. V. Protein coating composition targets nanoparticles to leaf stomata and trichomes. *Nanoscale* **2020**, *12*, 3630−3636.

(27) Kunst, L.; Samuels, A. L. Biosynthesis and secretion of plant cuticular wax. *Prog. Lipid Res.* **2003**, *42*, 51−80.

(28) Zhang, W. B.; Yu, X.; Wang, C. L.; Sun, H. J.; Hsieh, I. F.; Li, Y.; Dong, X. H.; Yue, K.; van Horn, R.; Cheng, S. Z. D. Molecular nanoparticles are unique elements for macromolecular science: From "Nanoatoms" to giant molecules. *Macromolecules* **2014**, *47*, 1221−1239.

(29) Cahyana, A. H.; Reza, A. I. Synthesis and characterization of Fe_3O_4 nanoparticles dispersed in paraffin as solvent. *AIP Conf. Proc.* **2018**, *2049*, No. 020047.

(30) Choudhuri, M.; Datta, A. Long-timescale dynamics of thiol capped Au nanoparticle clusters at the air-water interface. *AIP Conf. Proc.* **2014**, *1591*, 904−906.

(31) Braidwood, L.; Breuer, C.; Sugimoto, K. My body is a cage: mechanisms and modulation of plant cell growth. *New Phytol.* **2014**, *201*, 388−402.

(32) Leach, C. M.; Apple, J. D. Leaf surface electrostatics - Behavior of detached leaves of beans, maize, and other plants under natural conditions. *Phytopathology* **1984**, *74*, 704−709.

(33) Fernández, V.; Brown, P. H. From plant surface to plant metabolism: the uncertain fate of foliar-applied nutrients. *Front. Plant Sci.* **2013**, *4*, No. 289.

(34) Lević, L.; Tekić, M.; Djurić, M.; Kuljanin, T. $CaCl_2$, $CuSO_4$ and $AlCl_3$ & $NaHCO_3$ as possible pectin precipitants in sugar juice clarification. *Int. J. Food Sci.* **2007**, *42*, 609−614.

(35) van Schaik, J. W. J.; Kleja, D. B.; Gustafsson, J. P. Acid−base and copper-binding properties of three organic matter fractions isolated from a forest floor soil solution. *Geochim. Cosmochim. Acta* **2010**, *74*, 1391−1406.

(36) Lane, E. W.; Carlson, E. J. Some observations on the effect of particle shape on the movement of coarse sediments. *EOS, Trans. Am. Geophys. Union* **1954**, *35*, 453−462.

(37) Wang, G.; Sassa, K. Pore-pressure generation and movement of rainfall-induced landslides: effects of grain size and fine-particle content. *Eng. Geol.* **2003**, *69*, 109−125.

(38) He, J.; Zhang, L.; He, S. Y.; Rysere, E. T.; Li, H.; Zhang, W. Stomata facilitate foliar sorption of silver nanoparticles by *Arabidopsis thaliana*. *Environ. Pollut.* **2021**, *292*, No. 118448.

(39) Larue, C.; Castillo-Michel, H.; Sobanska, S.; Cecillon, L.; Bureau, S.; Barthes, V.; Ouerdane, L.; Carriere, M.; Sarret, G. Foliar exposure of the crop Lactuca sativa to silver nanoparticles: evidence

https://doi.org/10.1021/acs.jafc.1c07873
J. Agric. Food Chem. XXXX, XXX, XXX−XXX

for internalization and changes in Ag speciation. *J. Hazard. Mater.* **2014**, *264*, 98−106.

(40) Xiong, T.; Dumat, C.; Dappe, V.; Vezin, H.; Schreck, E.; Shahid, M.; Pierart, A.; Sobanska, S. Copper Oxide Nanoparticle Foliar Uptake, Phytotoxicity, and Consequences for Sustainable Urban Agriculture. *Environ. Sci. Technol.* **2017**, *51*, 5242−5251.

(41) Zhu, J.; Li, J.; Shen, Y.; Liu, S.; Zeng, N.; Zhan, X.; White, J. C.; Gardea-Torresdey, J.; Xing, B. Mechanism of zinc oxide nanoparticle entry into wheat seedling leaves. *Environ. Sci.: Nano* **2020**, *7*, 3901−3913.

(42) Zhao, J.; Ren, W.; Dai, Y.; Liu, L.; Wang, Z.; Yu, X.; Zhang, J.; Wang, X.; Xing, B. Uptake, distribution, and transformation of CuO NPs in a floating plant *Eichhornia crassipes* and related stomatal responses. *Environ. Sci. Technol.* **2017**, *51*, 7686−7695.

(43) Domínguez, E.; Heredia-Guerrero, J. A.; Heredia, A. The biophysical design of plant cuticles: an overview. *New Phytol.* **2011**, *189*, 938−949.

(44) Reed, H. S.; Hirano, E. The density of stomata in citrus leaves. *J. Agric. Res.* **1931**, *43*, 209−222.

(45) Jarecki, W.; Buczek, J.; Bobrecka-Jamro, D. Response of spring wheat to different soil and foliar fertilization. *J. Cent. Eur. Agric.* **2017**, *18*, 460−476.

(46) Jarecki, W.; Buczek, J.; Bobrecka-Jamro, D. The response of winter oilseed rape to diverse foliar fertilization. *Plant Soil Environ.* **2019**, *65*, 125−130.

(47) Gilbertson, L. M.; Pourzahedi, L.; Laughton, S.; Gao, X.; Zimmerman, J. B.; Theis, T. L.; Westerhoff, P.; Lowry, G. V. Guiding the design space for nanotechnology to advance sustainable crop production. *Nat. Nanotechnol.* **2020**, *15*, 801−810.

https://doi.org/10.1021/acs.jafc.1c07873
J. Agric. Food Chem. XXXX, XXX, XXX−XXX